crystals

MDPI

Article

Structural and Hirshfeld Surface Analysis of Thallium(I) and Indium(III) Complexes of a Soft Scorpionate Ligand

Kiyoshi Fujisawa [1,*], Ayaka Kuboniwa [1], Sang Loon Tan [2] and Edward R. T. Tiekink [2,*]

[1] Department of Chemistry, Ibaraki University, Mito, Ibaraki 310-8512, Japan
[2] Research Centre for Crystalline Materials, School of Medical and Life Sciences, Sunway University, Bandar Sunway 47500, Selangor Darul Ehsan, Malaysia; alant@sunway.edu.my
* Correspondence: kiyoshi.fujisawa.sci@vc.ibaraki.ac.jp (K.F.); edwardt@sunway.edu.my (E.R.T.T.)

Abstract: Two complexes containing a soft sulfur-substituted tris(pyrazolyl)hydroborate ligand, namely $[Tl^{I}(Tm^{tBu})]_2{\cdot}2H_2O$ and $[In^{III}(Tm^{tBu})_2](InCl_4)$, where Tm^{tBu} is the tris(3-*tert*-butyl-2-sulfanylidene-1*H*-imidazol-1-yl)hydroborate anion, have been characterized. The $\{TlS\}_2$ core of the former has the shape of a diamond. Each S atom of the Tm^{tBu} anion coordinates differently: one S is connected to one Tl atom, one bridges both Tl atoms, while the third S atom connects solely to the second Tl atom. The S_4 donor set defines a seesaw geometry. The independent H_2O molecule forms O–H···S and localized O–H···π(pyrazolyl) contacts. Flattened octahedral geometries defined by S_6 donor sets are noted for the two independent cations in $[In^{III}(Tm^{tBu})_2](InCl_4)$. In the crystal of $[Tl^{I}(Tm^{tBu})]_2{\cdot}2H_2O$, pyrazolyl-C–H···O(water) interactions connect the dimeric units into a linear supramolecular chain, chains pack without directional interactions between them. In the crystal of $[In^{III}(Tm^{tBu})_2](InCl_4)$, alternating rows of independent cations are interspersed by anions. The primary points of contact within a three-dimensional architecture are of the type In–Cl···π(pyrazolyl) and C–H···Cl. The assessment of the molecular packing was complemented by considering the calculated Hirshfeld surfaces and two-dimensional fingerprint plots (overall and delineated into individual contacts).

Keywords: thallium; indium; main group chemistry; tripodal ligand; thiol ligand; crystal structure; hydrogen bonding; Hirshfeld surface analysis

Citation: Fujisawa, K.; Kuboniwa, A.; Tan, S.L.; Tiekink, E.R.T. Structural and Hirshfeld Surface Analysis of Thallium(I) and Indium(III) Complexes of a Soft Scorpionate Ligand. *Crystals* **2023**, *13*, 745. https://doi.org/10.3390/cryst13050745

Academic Editor: Waldemar Maniukiewicz

Received: 10 April 2023
Revised: 26 April 2023
Accepted: 26 April 2023
Published: 29 April 2023

1. Introduction

Tripodal nitrogen-containing ligands, such as tris(pyrazolyl)hydroborate, have been utilized in the fields of inorganic and coordination chemistry [1,2]. One reason why the chemistry of this type of ligand has been studied so extensively relates to the fact that it is relatively facile to introduce substituents in the pyrazolyl rings with varying steric and electronic profiles. Recently, we developed transition metal complexes ligated by tris(pyrazolyl)hydroborate anion and/or their neutral analogues, i.e., tris(pyrazolyl)methanes, to determine how to control small molecule activation and their magnetism [3–6]. The history of the development and use of the tris(pyrazolyl)hydroborate ligand, often referred to as 'scorpionate', has been outlined by the founder of this chemistry, the late Prof. Swiatoslaw Trofimenko [7]. In Trofimenko's historical account, it was noted that new ligand architectures could also be obtained by the introduction of other heteroatoms, such as oxygen, sulfur, and phosphorus [7].

Thallium and indium are toxic metal *p*-block elements [8,9]. Recently, indium(III) oxide has been used as a transparent conductive coating on glass substrates in electroluminescent panels, i.e., ITO [9]. Thallium(I) and indium(III) are stable formal oxidation states and have electron configurations of $[Xe]4f^{14}5d^{10}6s^{2}6p^{0}$ and $[Kr]4d^{10}5s^{0}5p^{0}$, respectively. With respect to tripodal ligands, the introduction of sulfur gives rise to S_3-tripod type ligands, e.g., tris(3-*tert*-butyl-2-sulfanylidene-1*H*-imidazol-1-yl)hydroborate (denoted Tm^{tBu}) (Figure 1, left; R = tBu), being a soft tris(pyrazolyl)hydroborate derivative that readily

complexes heavy metal *p*-block elements, such as bismuth(III) [10]; for relevant reviews of the coordination chemistry of *p*-block elements with soft S_3-type ligands, see [11–13].

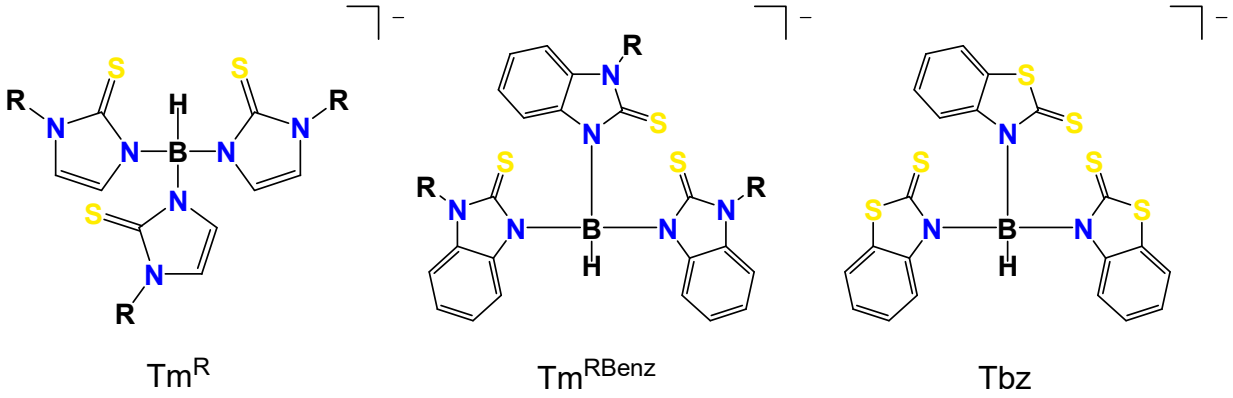

Figure 1. Schematic drawing of the ligands: tris(3-R-2-sulfanylidene-1*H*-imidazol-1-yl)hydroborate (Tm^R), tris(3-R-2-sulfanylidene-1*H*-benzimidazol-1-yl)hydroborate (Tm^{RBenz}), and tris(2-sulfanylidene-1*H*-benzothiazol-1-yl)hydroborate (Tbz).

In continuation of previous work, the crystal and molecular structures, as well as a detailed analysis of the calculated Hirshfeld surfaces, are described for thallium(I), $[Tl^{I}(Tm^{tbu})]_2$, characterized as a dihydrate, and indium(III), $[In^{III}(Tm^{tBu})_2]^+$, complexes ligated by the same soft tripod sulfur-containing type ligand employed in an earlier study [10], namely Tm^{tBu}. This work compliments the literature precedents of thallium(I), thallium(III), indium(I), and indium(III) complexes ligated by tris(3-R-2-sulfanylidene-1*H*-imidazol-1-yl)hydroborate (Tm^R), tris(3-R-2-sulfanylidene-1*H*-benzimidazol-1-yl)hydroborate (Tm^{RBenz}), and tris(2-sulfanylidene-1*H*-benzothiazol-1-yl)hydroborate (Tbz) ligands (Figure 1)—thallium(I): $[Tl(Tm^{MeBenz})]$ [14], $[Tl(Tm^{tBuiBenz})]\cdot C_6H_6$ [14], $[Tl(Tm^{tBu})]_2$ [15], $[Tl(Tm^{Ph})]_2$ [16], and $[Tl(Tbz)]_\infty\cdot CH_2Cl_2$ [17]; thallium(III): $[Tl(Tm)_2](TlI_4)$ [18], $[Tl(Tm)_2](I)$ [14], and $[Tl(Tm^{Ph})_2](ClO_4)$ [16]; indium(I): $[In(Tm^{tBu})]$ [15], $[In(Tm^{tBu})\{B(C_6F_5)_3\}]$ [15], $[In(Tm^{tBu})(\kappa^2\text{-}S_4)]$ [15]; and $[In(Tm^{tBu})_2](I)$ [15]; indium(III): $[In(Tm^{Ad})_2](InI_4)$ [19], $[In(Tm^{Ad})(\kappa^2\text{-}mim^{Ad})](Cl)$ [19], $[In(Tm^{Ad})\{B(C_6F_5)_3\}](Cl)$ [19], $[In(Tm^{tBu})]$ [15], and $[In(Tm^{Me})_2](I)$ [20].

2. Materials and Methods

2.1. Chemicals and Instrumentation

The preparation and handling of the two complexes were performed under an argon atmosphere using standard Schlenk tube techniques. Dichloromethane was carefully purified by refluxing and distilling under an argon atmosphere over phosphorous pentoxide. Heptane, toluene, and tetrahydrofuran were carefully purified by refluxing and distilling under an argon atmosphere over sodium benzophenone ketyl [21]. Dry ethanol was purchased from Wako Pure Chemical Ind. Ltd. and deoxygenated by purging with argon gas. Deuteriochloroform was obtained from Cambridge Isotope Laboratories, Inc. (Tewksbury, MA, USA). Other reagents were commercially available and used without further purification. The potassium salt of tris(3-*tert*-butyl-2-sulfanylidene-1*H*-imidazol-1-yl)hydroborate (KTm^{tBu}) was prepared by published methods [22–25].

2.2. Instrumentation

IR spectra (4000–400 cm^{-1}) were recorded as KBr pellets using a JASCO FT/IR-6300 spectrophotometer (JASCO, Tokyo, Japan). Raman spectra (4000–200 cm^{-1}) were measured as powders on a JASCO RFT600 spectrophotometer with a YAG laser 650 mW (JASCO, Tokyo, Japan). Abbreviations used in the description of vibrational data are as follows: s, strong; m, medium; w, weak. ^{1}H-NMR (500 MHz) and ^{13}C-NMR (125 MHz) spectra were obtained on a Bruker AVANCE III-500 NMR spectrometer at room temperature (298 K) in $CDCl_3$ (Bruker Japan, Yokohama, Japan). ^{1}H and ^{13}C chemical shifts were reported as δ

values relative to residual solvent peaks (7.26 and 77.16 ppm, respectively). UV–Vis spectra (solution CH_2Cl_2, 1050–250 nm) were recorded on an Agilent 8453 UV–visible spectroscopy system (Agilent, Tokyo, Japan). The elemental analyses (C, H, and N) were performed by the Chemical Analysis Center of Ibaraki University.

2.3. Preparation of Complexes

2.3.1. $[Tl(Tm^{tBu})]_2{\cdot}2H_2O$

A solution of $K(Tm^{tBu})$ (0.5114 g, 0.991 mmol) in dichloromethane (15 mL) was added to a solution of thallium(I) acetate (0.2649 g, 1.006 mmol) in degassed ethanol (10 mL). After allowing the reaction to proceed overnight, the solvent was removed under reduced pressure, and the resulting solid was extracted by dichloromethane (15 mL). Colorless crystals were obtained by slow evaporation from a saturated dichloromethane/heptane (1:1 v/v) solution and were characterized crystallographically as $[Tl(Tm^{tBu})]_2{\cdot}2H_2O$ (0.2820 g, 0.410 mmol, yield: 41%). Elemental analysis (bulk material): Anal. Calcd. for $[Tl(Tm^{tBu})]{\cdot}1/3H_2O$: C 36.66, H 5.08, N 12.22%; Found: C 36.43, H 4.90 N 11.93%. IR (KBr, cm^{-1}): 3147 w ν(C–H), 2975 m ν(C–H), 2922 w ν(C–H), 2455 w ν(B–H), 1626 m, 1560 w, 1407 m, 1396 m, 1357 s, 1273 m, 1199 s, 1165 m, 1099 m, 981 w, 737 w, 715 m, 682 m. Raman (cm^{-1}): 3188 w (C–H), 3145 w ν(C–H), 2979m ν(C–H), 2959 m ν(C–H), 2922m ν(C–H), 2445 w ν(B–H), 1564 s, 1458 m, 1358 s, 1258 w, 1226 w, 1153 w, 1099 w, 1058 w, 1026 w, 931 w, 821 w, 716 w, 611 w, 564 w, 407 w, 314 w. ^{1}H NMR ($CDCl_3$, 298 K): 1.79 (s, 27H, CH_3), 6.12 (3H, imidazole H), 6.86 (3H, imidazole H). ^{13}C NMR ($CDCl_3$, 298 K): 28.7 (CCH_3), 58.5 (CCH_3), 115.9 (imidazole C_4 or C_5), 123.1 (imidazole C_4 or C_5), 161.2 (imidazole C=S). UV–vis (CH_2Cl_2, 298 K; λ_{max}, nm (ε, $M^{-1}cm^{-1}$)): 270 (20,700).

2.3.2. $[In(Tm^{tBu})_2](InCl_4)$

A solution of $[Tl(Tm^{tBu})]_2{\cdot}2H_2O$ (0.0706 g, 0.050 mmol) in dichloromethane (5 mL) was added to a solution of $InCl_3{\cdot}4H_2O$ (0.0294 g, 0.100 mmol) in tetrahydrofuran (5 mL). After allowing the reaction to proceed overnight, the solvent was removed under reduced pressure, and the resulting solid was extracted with dichloromethane (10 mL). Colorless crystals were obtained by slow evaporation from a saturated dichloromethane/toluene (1:1 v/v) solution as $[In(Tm^{tBu})_2](InCl_4)$ (0.0586 g, 0.044 mmol, yield: 88%). Elemental analysis: Anal. Calcd. for $[In(Tm^{tBu})_2](InCl_4)$: C 38.03, H 5.17, N 12.67%; Found: C 38.04, H 5.09 N 12.33%. IR (KBr, cm^{-1}): 3181w ν(C–H), 3147 w ν(C–H), 2979 m ν(C–H), 2928 m ν(C–H), 2423 w ν(B–H), 1567 w, 1480 m,1420 s, 1398 m, 1357 s, 1308 m, 1260 w, 1228 m, 1098 s, 1177 s, 1072 w, 822 w, 768 w, 732 m, 687 m, 590 w, 552 w, 496 w, 457 w. Raman (cm^{-1}): 3184 w ν(C–H), 3152 w ν(C–H), 3111 w ν(C–H), 2986 m ν(C–H), 2928 m ν(C–H), 2425 w ν(B–H), 1568 m, 1450 w, 1431 w, 1359 s, 1307 w, 1255 w, 1248 w, 1073 w, 1041 w, 986 w, 932 w, 825 w, 738 w, 637 w, 590 w, 401 w, 320 w. ^{1}H NMR ($CDCl_3$, 298 K): 1.74 (*s*, 9H, C*H*$_3$), 1.79 (*s*, 18H, C*H*$_3$), 6.82 (*d*, 1H, *J* = 2.0 Hz, imidazole *H*), 6.89 (*d*, 2H, *J* = 2.0 Hz, imidazole *H*), 7.08 (*d*, 1H, *J* = 2.0 Hz, imidazole *H*), 7.12 (*d*, 2H, *J* = 2.0 Hz, imidazole *H*). ^{13}C NMR ($CDCl_3$, 298 K): 29.9 (CCH_3), 30.1 (CCH_3), 60.1 (*C*CH_3), 60.8 (*C*CH_3), 118.3 (imidazole C_4 or C_5), 123.9 (imidazole C_4 or C_5), 153.2 (imidazole *C*=S). UV–vis (CH_2Cl_2, 298 K; λ_{max}, nm (ε, $M^{-1}cm^{-1}$)): 268 (17,900), 307 (8000).

2.4. X-ray Crystallography

Colorless crystals of $[Tl(Tm^{tBu})]_2{\cdot}2H_2O$ and $[In(Tm^{tBu})_2](InCl_4)$ were coated with Paratone-N oil (Hampton Research, Aliso Viejo, CA, USA) and mounted on a Dual-Thickness MicroLoop LD (200 μM) (MiTeGen, New York, NY, USA). X-ray intensity data were measured at T = 178 K on a Rigaku/Oxford Diffraction Rigaku XtaLAB P200 diffractometer (Rigaku Oxford Diffraction, Oxfordshire, UK) fitted with MoKα radiation (λ = 0.71073 Å) so that 100% data completeness was achieved at θ_{max} = 25.2°. Data reduction, including empirical absorption correction, was accomplished with CrysAlisPro (Rigaku Oxford Diffraction, Oxfordshire, UK) [26]. The structures were solved by direct methods [27] and refined (anisotropic displacement parameters and C-bound H atoms in the riding model approximation) on F^2 [28]. For **2**, the positions of the water-bound H

atoms were idealized based on chemically reasonable positions with the O–H and H···H distances initially refined with restraints 0.840 ± 0.001 and 1.30 ± 0.001 Å, respectively, and fixed at these values in the final cycles of refinement. A weighting scheme of the form $w = 1/[\sigma^2(F_o^2) + (aP)^2 + bP]$, where $P = (F_o^2 + 2F_c^2)/3$), was applied toward the latter stages of each refinement. At the conclusion of each refinement, relatively large residual electron density peaks were noted; details are given in the respective CIFs. The molecular structure diagrams were generated with ORTEP for Windows [29] with 50% displacement ellipsoids, and the packing diagrams were drawn with DIAMOND [30]. Additional data analysis was made with PLATON [31]. Crystal data and refinement details are given in Table 1.

Table 1. Crystallographic data and refinement details for $[Tl(Tm^{tBu})]_2{\cdot}2H_2O$ and $[In(Tm^{tBu})_2](InCl_4)$.

Complex	$[Tl(Tm^{tBu})]_2{\cdot}2H_2O$	$[In(Tm^{tBu})_2](InCl_4)$
Formula	$C_{42}H_{68}B_2N_{12}S_6Tl_2$, $2(H_2O)$	$C_{42}H_{68}B_2InN_{12}S_6$, $InCl_4$
Molecular weight	1399.86	1326.50
Crystal size/mm^3	0.03 × 0.10 × 0.13	0.13 × 0.22 × 0.26
Colour	colorless	colorless
Crystal system	triclinic	triclinic
Space group	$P\bar{1}$	$P\bar{1}$
a/Å	9.5421(2)	11.1900(1)
b/Å	11.8656(2)	11.4449(2)
c/Å	14.5839(3)	23.2153(3)
a/°	67.963(2)	94.421(1)
β/°	71.203(2)	92.606(1)
γ/°	73.428(2)	90.262(1)
V/Å^3	1423.33(6)	2961.14(7)
Z	1	2
D_c/g cm^{-3}	1.633	1.488
μ/mm^{-1}	5.918	1.212
Measured data	48,875	101474
θ range/°	2.5–29.9	2.6–29.8
Unique data	7633	15775
Observed data ($I \geq 2.0\sigma(I)$)	6786	14551
No. of parameters	298	616
R, obs. data; all data	0.032; 0.038	0.028; 0.030
a; b in weighting scheme	0.055; 1.294	0.041; 2.674
Rw, obs. data; all data	0.085; 0.087	0.075; 0.076
Range of residual electron density peaks/eÅ^{-3}	−1.38–2.58	−0.78–1.76

3. Results and Discussion

3.1. Synthesis and Characterization

The reactions of the ligand $K(Tm^{tBu})$ [22–25] with one equivalent of thallium(I) acetate (TlOAc) were carried out at room temperature, and single crystals of the thallium(I) complex, formulated as $[Tl(Tm^{tBu})]_2{\cdot}2H_2O$, were obtained by slow evaporation of a dichloromethane/ethanol solution at room temperature (Figure 2). The indium(III) complex, $[In(Tm^{tBu})_2](InCl_4)$, was obtained by the reaction of $[Tl(Tm^{tBu})_2]$ with indium(III) chloride $InCl_3{\cdot}4H_2O$. The colorless crystals were obtained from the mixed solution of the saturated dichloromethane/toluene solution (Figure 2).

The expected signals in IR and Raman spectra were obtained for each $[Tl(Tm^{tBu})]_2$ and $[In(Tm^{tBu})_2](InCl_4)$. Noteworthy were the B–H stretching bands at 2455 cm^{-1} for $[Tl(Tm^{tBu})]_2$ and 2423 cm^{-1} for $[In(Tm^{tBu})_2](InCl_4)$, which were clearly evident and red-shifted compared to 2480 cm^{-1} for $K(Tm^{tBu})$ [25] (Figures S1 and S2 of the Supplementary Materials). The ^{1}H-and ^{13}C NMR spectra of $[Tl(Tm^{tBu})]_2$ in $CDCl_3$ occurred at chemical shifts identical to those of KTm^{tBu} (Figures S3–S5 of the Supplementary Materials). For $[In(Tm^{tBu})_2](InCl_4)$, all chemical shifts in the ^{1}H-NMR, and all those except for C=S carbon shifts in the ^{13}C-NMR, were clearly split due to the different structural arrangements,

i.e., occupying equatorial and axial coordination sites. The UV–Vis absorption spectra of $[Tl(Tm^{tBu})]_2$ and $[In(Tm^{tBu})_2](InCl_4)$ were also measured (Figure S6 of the Supplementary Materials). Two characteristic absorption bands at 268 and 307 nm were observed for $[In(Tm^{tBu})_2](InCl_4)$, but for $[Tl(Tm^{tBu})]_2$, only a band at 261 nm was noted. From this observation, the high-energy bands at 260 and 268 nm band were assigned to a ligand Tm^{tBu}-based absorption, and the low-energy band for $[In(Tm^{tBu})_2](InCl_4)$ is metal centered. For more detailed assignments, computational chemistry calculations are required, which are beyond the scope of this study. The ^{1}H-NMR and UV–Vis spectroscopy results indicate that the structures remained intact in the solution state.

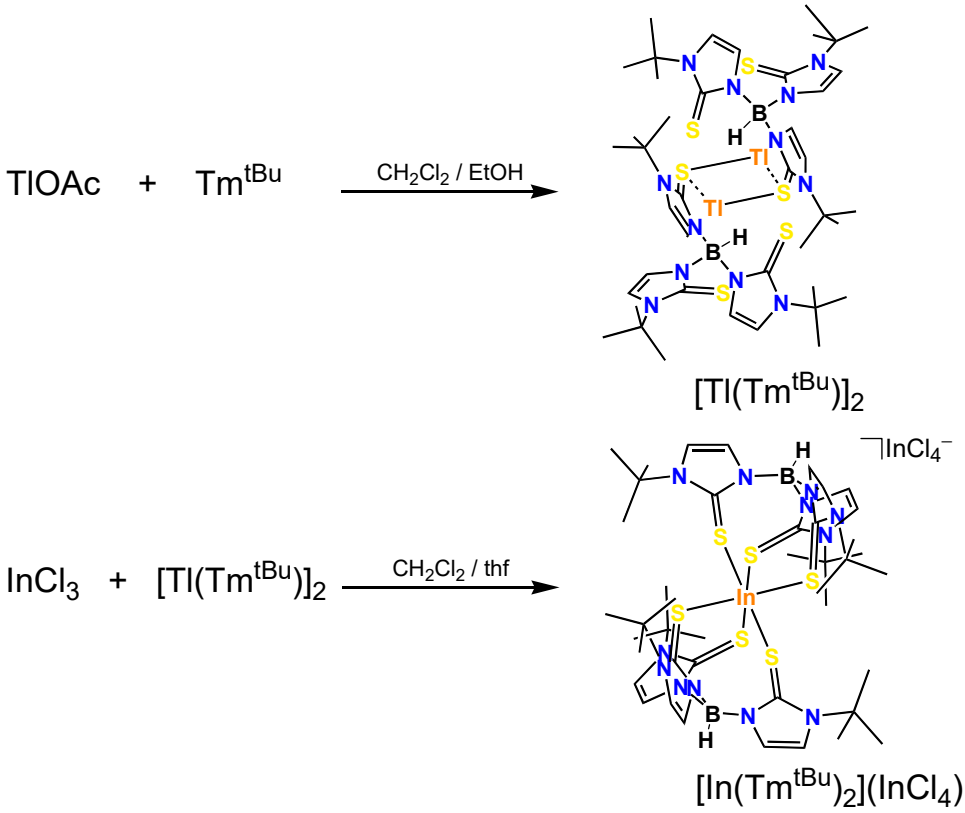

Figure 2. Syntheses of thallium(I) complex, $[Tl(Tm^{tBu})]_2$, and indium(III) complex, $[In(Tm^{tBu})_2](InCl_4)$.

3.2. Crystal and Molecular Structures

3.2.1. Molecular Structures

The crystallographic asymmetric unit of $[Tl^I(Tm^{tBu})]_2{\cdot}2H_2O$ comprises one-half of a dimeric complex molecule, being located about a center of inversion and a water molecule of crystallization. The complex molecule is shown in Figure 3a and comprises a central, diamond-shaped core with almost equivalent Tl1–S1, $S1^i$ bond lengths (Table 2). The four-coordinate geometry for thallium is completed by the thione-S2 and symmetry-related thione-$S3^i$ atoms. An indication of the coordination geometry defined by the S_4 donor set is τ_4, which is computed from $[360 - (\alpha + \beta)]/141$, where α and β are the two widest angles subtended at the thallium(I) atom [32]. In this case, $\tau_4 = 0.63$, which corresponds to a seesaw geometry ($\tau_4 = 0.64$); the widest angle corresponds to S2–Tl1–$S3^i$, i.e., 156.32(3)°. The Tm^{tBu} ligand is therefore tetra-coordinating, bridging two thallium(I) centers. A curious feature of the molecular structure is a close intramolecular B–H···ring centroid (Tl_2S_2) separation of 2.17 Å. This is a consequence of the coordination mode of the Tm^{tBu} ligand and has been observed in literature analogs, e.g., in the benzene mono-solvate of $[Tl(Tm^{tBu})]_2$ [15] and in $[Tl(Tm^{Ph})]_2$, as its chloroform mono-solvate [16], each of which features the same κ^3 coordination mode as described above but with variations in the magnitudes of the Tl–S1 bond lengths.

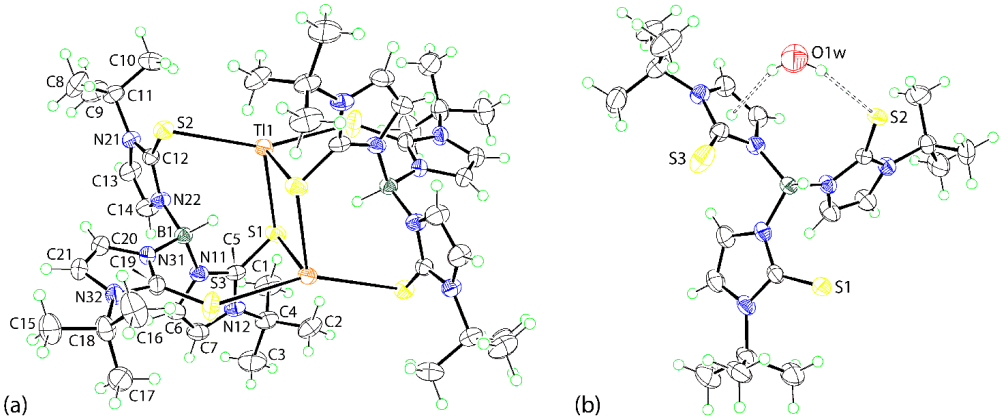

Figure 3. (**a**) Molecular structure of the complex molecule in $[Tl(Tm^{tBu})]_2 \cdot 2H_2O$, showing atom labeling scheme and displacement ellipsoids at the 50% probability level, and (**b**) detail of the supramolecular molecular association (dashed lines) involving the water molecule. Unlabeled atoms in (**a**) are related by the symmetry operation $2 - x, 1 - y, - z$.

Table 2. Selected geometric parameters (Å, °) for $[Tl(Tm^{tBu})]_2 \cdot 2H_2O$.

Parameter	Value	Parameter	Value
Tl1–S1	3.0408(9)	S1–Tl1–S3^{i}	82.04(3)
Tl1–S2	3.1696(9)	S2–Tl1–S1^{i}	91.89(2)
Tl1–S1^{i} [a]	2.9993(10)	S2–Tl1–S3^{i}	156.32(3)
Tl1–S3^{i} [a]	3.2764(11)	S1^{i}–Tl1–S3^{i}	104.23(3)
C5–S1	1.721(4)	Tl1–S1–Tl1^{i}	86.10(2)
C12–S2	1.700(3)	Tl1–S1–C5	120.26(12)
C19–S3	1.694(4)	Tl1–S2–C12	83.37(12)
S1–Tl1–S2	114.53(2)	Tl1–S1^{i}–C5^{i}	86.11(12)
S1–Tl1–S1^{i} [a]	93.90(2)	Tl1–S3^{i}–C19^{i}	127.75(14)
(N11,N12,C5-C7)/(N21,N22,C12-C14)	88.2(3)	(N21,N22,C12-C14)/(N31,N32,C19-C21)	78.7(3)
(N11,N12,C5-C7)/(N31,N32,C19-C21)	83.2(3)		

[a] symmetry operation: $2 - x, - y, - z$.

As highlighted in Figure 3b, the water molecule of crystallization is closely associated with the complex molecule, forming a hydrogen bond to the thione-S2 atom and close contact with the N31-pyrazolyl ring; see Table 3 for the geometric parameters defining these interactions. The H2w···ring centroid separation is 2.47 Å, with the closest contact to a specific atom within the ring being 2.45 Å, i.e., the C19 atom with the next closest interaction, i.e., 2.60 Å with N31, and the longest separation of 2.97 Å with C21. This pattern indicates that the interaction is best described as a localized H2w···π interaction [33].

Table 3. Geometric parameters (Å, °) characterizing the specified intermolecular contacts operating in the crystal of $[Tl(Tm^{tBu})]_2 \cdot 2H_2O$ [a].

A	H	B	H···B	A···B	A–H···B	Symmetry Operation
O1w	H1w	S2	2.47	3.2779(10)	160	x, y, z
O1w	H2w	Cg (1)	2.47	3.2816(18)	161	x, y, z
C13	H13	O1w	2.46	3.214(5)	136	$-1 + x, y, z$

[a] Cg(1) is the ring centroid of the (N31,N32,C19-C21) ring.

The asymmetric-unit of $[In^{III}(Tm^{tBu})_2](InCl_4)$ comprises two independent complex cations, each disposed about a center of inversion, and a $InCl_4^-$ anion; the molecular structures are shown in Figure 4a–c. Focusing on the In1-containing molecule, the In1 atom is coordinated by two tripodal Tm^{tBu} ligands to define a soft S_6 donor set, which defines an octahedral geometry. The geometry is slightly flattened, as the In1–S1 bond length of

2.5682(4) Å is systematically shorter than the In1–S2, S3 bond lengths of 2.6597 (4) and 2.6429(4) Å (Table 4). Despite this difference, the C5–S1 bond lengths are equal within experimental error. Otherwise, the deviations from the ideal octahedral geometry are small, as noted from the relevant angles included in Table 4. As highlighted by the dihedral angles between the pyrazolyl rings listed in Table 4 and the overlay diagram of Figure 4d, there is close agreement between the independent molecules. This observation notwithstanding, there are notable differences in the In–S bond lengths. Thus, in the first independent cation of $[In^{III}(Tm^{tBu})_2](InCl_4)$, one In–S bond length is 0.07–0.10 Å shorter than the others, whereas in the second independent cation, the differential between the In–S bond lengths is significantly smaller, i.e., the difference between the shortest and longer bond lengths is now 0.02–0.08 Å.

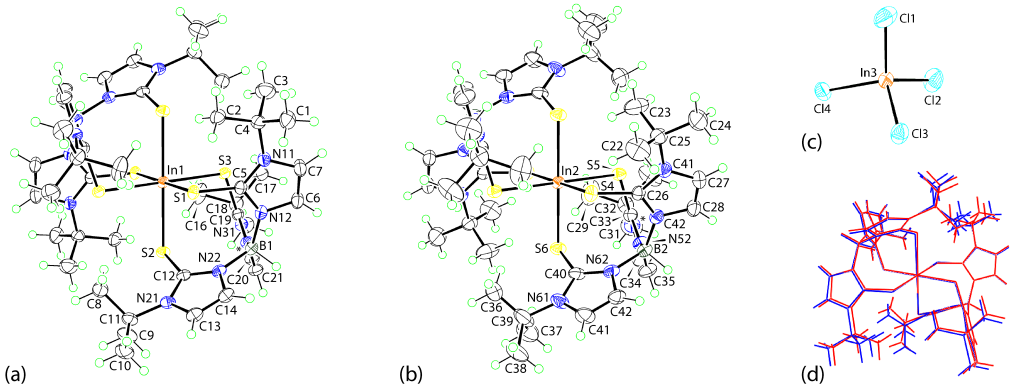

Figure 4. Molecular structure diagrams for $[In(Tm^{tBu})_2](InCl_4)$: (**a**) through (**c**) molecular structures of the independent In1- and In2-containing cations, and In3-anion, respectively, showing atom labeling schemes and displacement ellipsoids at the 50% probability level. (**a**) The N32 atom is indicated by an asterisk, and the C15 atom is not labeled. (**b**) The N51 atom is indicated by an asterisk, and the C30 atom is not labeled. The In atoms in (**a**) and (**b**) are located at crystallographic centers of inversion with the unlabeled atoms generated by the application of symmetry operations $1 - x, 1 - y, - z$ and $1 - x, 1 - y, 1 - z$. (**d**) overlay diagram of the In1- and In2-containing cations shown as red and blue images, respectively. The cations have been overlapped so that the S_3 faces are coincident.

Table 4. Selected geometric parameters (Å, °) for $[In(Tm^{tBu})_2](InCl_4)$.

Parameter	Value	Parameter	Value
In1–S1	2.5682(4)	In2–S4	2.6110(4)
In1–S2	2.6597(4)	In2–S5	2.6709(5)
In1–S3	2.6429(4)	In2–S6	2.5905(5)
C5–S1	1.7236(17)	C26–S4	1.7223(19)
C12–S2	1.7279(17)	C33–S5	1.7249(19)
C19–S3	1.7253(17)	C40–S6	1.725(2)
S1–In1–S2	91.715(13)	S4–In2–S5	92.567(14)
S1–In1–S3	93.179(13)	S4–In2–S6	95.416(15)
S2–In1–S3	92.142(13)	S5–In2–S6	89.139(15)
In1–S1–C5	105.90(6)	In2–S4–C26	109.61(6)
In1–S2–C12	107.64(6)	In2–S5–C33	106.11(7)
In1–S3–C19	106.57(6)	In2–S6–C40	106.41(7)
(N11,N12,C5-C7)/(N21,N22,C12-C14)	83.99(11)	(N41,N42,C26-C28)/(N21,N22,C12-C14)	82.84(12)
(N11,N12,C5-C7)/(N31,N32,C19-C21)	89.18(11)	(N41,N42,C26-C28)/(N51,N52,C33-C35)	88.91(13)
(N21,N22,C12-C14)/(N31,N32,C19-C21)	87.98(11)	(N51,N52,C33-C35)/(N61,N62,C40-C42)	84.43(13)

There are several literature precedents for $[In(Tm^{tBu})_2](InCl_4)$, including $[In(Tm^{tBu})_2]^+$ characterized as the Cl^- as an acetonitrile tri-solvate [15], and I^- as a benzene mono-solvate, salts [15], along with $[In(Tm^{Me})_2]^+$ characterized as the I^- salt as a diethyl ether mono- and dimethylformamide di-solvate [20]. While the indium(III) centers in all three literature

complex cations exist within S_6 donor sets, the symmetries of these vary. Thus, in the chloride salt of $[In(Tm^{tBu})_2]^+$, each indium atom of the two independent molecules sits on an inversion center; in the iodide salt, the indium atom is located on a three-fold inversion center, implying that all In–S lengths are equivalent. The $[In(Tm^{Me})_2]^+$ cation is located on an inversion center.

3.2.2. Molecular Packing

The water molecule of solvation in $[Tl(Tm^{tBu})]_2{\cdot}2H_2O$ proves pivotal in assembling the dimeric molecules into a supramolecular chain along the *a*-axis, as shown in Figure 5a. Thus, the water molecule forms O–H···π(pyrazolyl) and O–H···S interactions, as shown in detail in Figure 3b, with the bay region of the Tm^{tBu} ligand. At the same time, the water-O atom accepts an interaction from a pyrazolyl-C–H atom; see Table 3 for geometric parameters. Chains pack in the crystal without directional interactions between them, as highlighted in the unit cell diagram of Figure 5b.

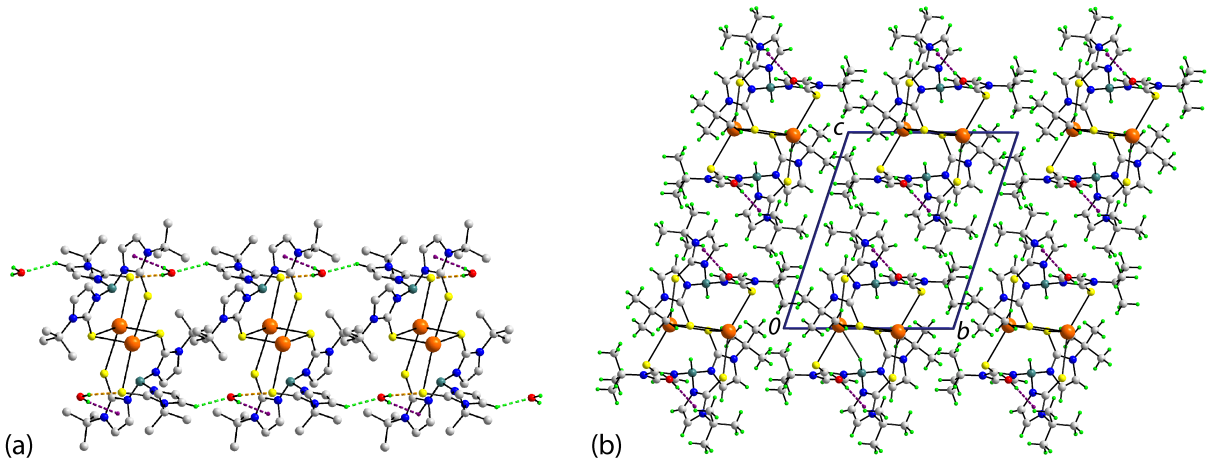

Figure 5. Molecular packing in the crystal of $[Tl(Tm^{tBu})]_2{\cdot}2H_2O$: (**a**) supramolecular chain aligned along the *a*-axis (non-participating H atoms are omitted) and (**b**) a view of the unit cell contents viewed in projection down the **a**-axis. The O–H···π(pyrazolyl), O–H···S and C–H···O contacts are highlighted as purple, orange and bright-green dashed lines, respectively.

A view of the unit cell contents for $[In(Tm^{tBu})_2](InCl_4)$ is shown in Figure 6. Globally, when viewed down the *b*-axis, molecules of In1- and In2-containing cations and $[InCl_4]^-$ anions stack in columns along this axis. The cations align in rows along the *a*-axis, and the rows alternate in an ···ABA··· fashion down the *c*-axis. Interspersed between rows are the $[InCl_4]^-$ anions, and these are pivotal in providing links between the constituent cations. The primary mode of interaction is via C–H···Cl contacts of the type pyrazolyl-C–H···Cl and methyl-C–H···Cl; for geometric parameters characterizing these interactions, refer to Table 5. The anion also forms an In–Cl···π(pyrazolyl) interaction, which is discussed in more detail in Section 3.3.

Table 5. Geometric parameters (Å, °) characterizing the specified intermolecular contacts operating in the crystal of $[In(Tm^{tBu})_2](InCl_4)$ [a].

A	H	B	H···B	A···B	A–H···B	Symmetry Operation
C21	H21	Cl1	2.85	3.723 (2)	154	$x, -1+y, z$
C41	H41	Cl3	2.83	3.773 (2)	174	$1-x, -y, 1-z$
C42	H42	Cl4	2.81	3.562 (2)	137	$1-x, -y, 1-z$
C1	H1b	Cl4	2.83	3.797 (2)	168	x, y, z
In3	Cl1	Cg(1)	3.7819 (11)	6.0631 (9)	162.17 (3)	$x, -1+y, z$

[a] Cg(1) is the ring centroid of the (N21,N22,C12-C14) ring.

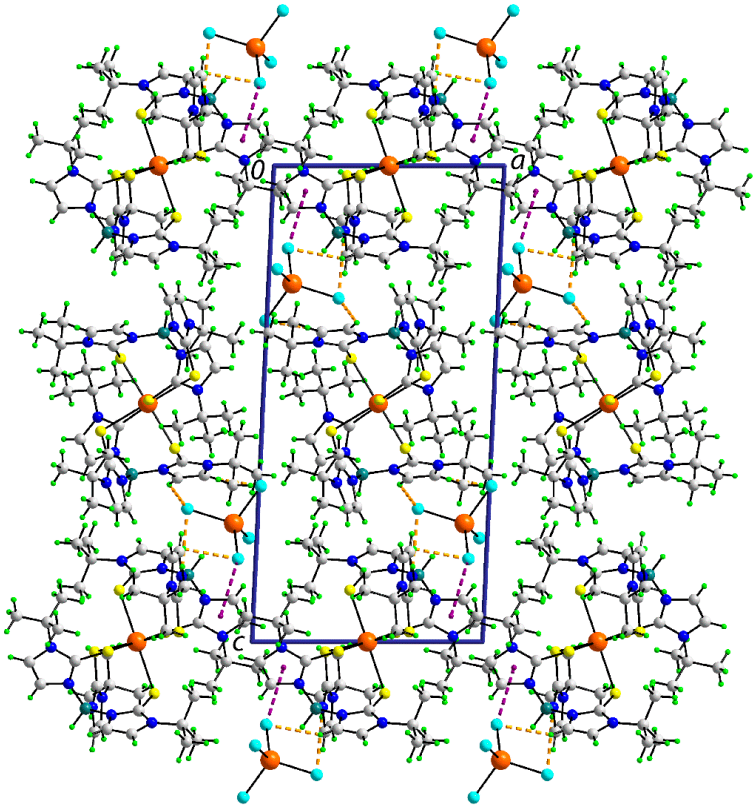

Figure 6. A view of the unit cell contents for $[In(Tm^{tBu})_2](InCl_4)$ viewed in projection down the *b*-axis. The In–Cl···π(pyrazolyl) and C–H···Cl contacts are highlighted as purple and orange dashed lines, respectively.

3.3. Hirshfeld Surface Analysis

To further understand the nature of the contacts between molecules in their respective crystals, an analysis of the calculated Hirshfeld surfaces was conducted employing *Crystal Explorer 17* [34] following established protocols [35]. The analysis shows that there are some close contacts present in each crystal, as evident from the red spots of various intensity observed on the respective d_{norm} maps indicating contact distances shorter than the sum of van der Waals radii [36].

For $[Tl(Tm^{tBu})]_2 \cdot 2H_2O$, the d_{norm} map of the $Tl(Tm^{tBu})$ fragment shows several red spots of moderate to strong intensity (Figure 7), which can be attributed to O1w–H1w···S2, O1w–H2w···C19(π), and C13–H13···O1w close contacts, with the respective contact distances being 2.37, 2.35, and 2.34 Å compared to the respective sums of the van der Waals radii (ΣvdW) of 2.89, 2.79, and 2.61 Å for H···S, H···C, and H···O (Table 6).

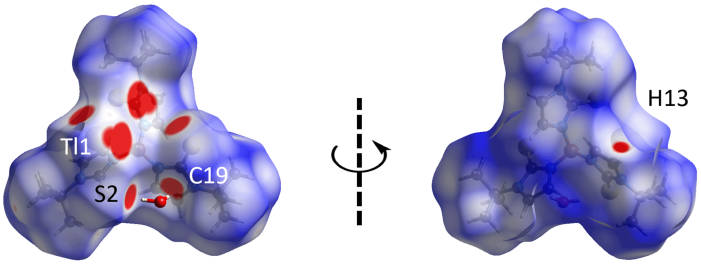

Figure 7. The two views of the d_{norm} Hirshfeld surface mapping for the $Tl(Tm^{tBu})$ fragment of $[Tl(Tm^{tBu})]_2 \cdot 2H_2O$ within the range −0.1027 to 1.3365 arbitrary units, highlighting close contacts as red regions on the surfaces with their intensity relative to the contact distance.

Table 6. d_{norm} contact distances (adjusted to neutron values) of intermolecular interactions identified in the crystals of $[Tl(Tm^{tBu})]_2 \cdot 2H_2O$ and $[In(Tm^{tBu})_2](InCl_4)$, as computed through the Hirshfeld surface analysis and in comparison to the corresponding sum of van der Waals radii (ΣvdW).

Contact	Distance (Å)	ΣvdW (Å)	Δ(ΣvdW—Distance)	Symmetry Operation
$[Tl(Tm^{tBu})]_2 \cdot 2H_2O$				
H1w···S2	2.37	2.89	0.52	x, y, z
H2w···C19	2.35	2.79	0.44	x, y, z
H13···O1w	2.34	2.61	0.27	$-1+x, y, z$
$[In(Tm^{tBu})_2](InCl_4)$				
H41···Cl3	2.40	2.84	0.44	$1-x, -y, 1-z$
H21···Cl1	2.49	2.84	0.35	$x, -1+y, z$
H37c···H30a	1.93	2.18	0.25	$1+x, y, z$
H42···Cl4	2.72	2.84	0.12	$1-x, -y, 1-z$
H1b···Cl4	2.73	2.84	0.11	x, y, z
H6···Cl4	2.78	2.84	0.06	x, y, z
H35···C19	2.76	2.79	0.03	x, y, z

Hirshfeld surface analysis was also performed for the central thallium atom (Figure 8). The d_{norm} map displays several weak to intense red spots indicating additional intramolecular interactions between B1–H1···Tl (d_{norm} distance = 2.69 Å vs. ΣvdW = 3.05 Å) and C10–H10a···Tl (d_{norm} distance = 3.00 Å vs. ΣvdW = 3.05 Å) on top of S1···Tl, S2···Tl and S3···Tl contacts, as described above.

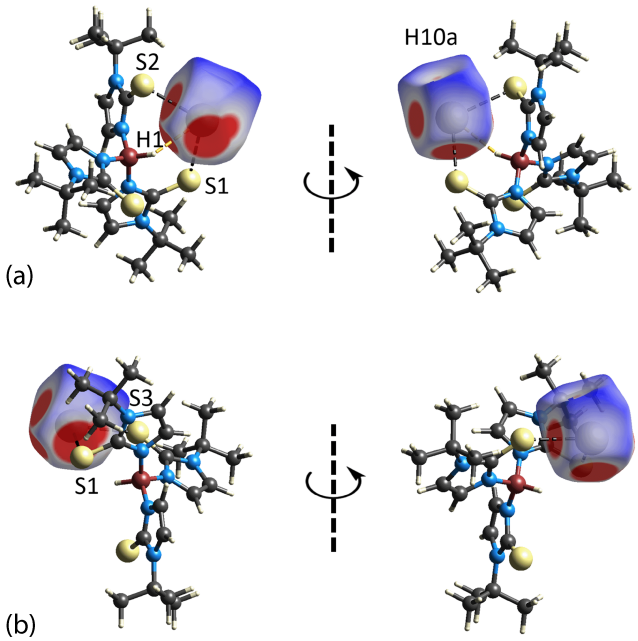

Figure 8. The two views of the d_{norm} Hirshfeld surface mapping within the range −0.1027 to 1.3365 arbitrary units for the thallium center in $[Tl(Tm^{tBu})]_2 \cdot 2H_2O$, showing the coordination modes of the metal with two Tm^{tBu} ligands of different symmetry: (**a**): x, y, z and (**b**) $2-x, 1-y, -z$.

The d_{norm} analysis was also conducted for each of the In1- or In2-containing cations and In3-anion in $[In(Tm^{tBu})_2](InCl_4)$ (Figure 9). A number of red spots with moderate intensity are observed for close contacts comprising C41–H41···Cl3, C21–H21···Cl1, and C42–H42···Cl4, in accordance with those interactions identified through the geometric analysis conducted with PLATON [31]. However, additional contacts were noted through the d_{norm} map arising from H37c···H30a, with moderate intensity, as well as from C1–H1b···Cl4, C6–H6···Cl4, and C35–H35···C19 with weak intensity. Table 6 summarizes these contacts and compares the separation distances with the respective van der Waals radii.

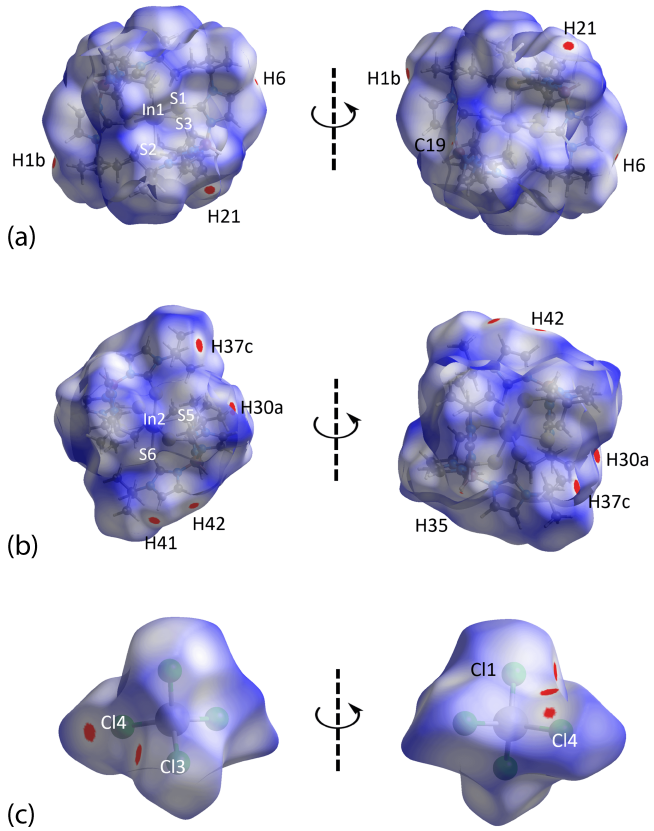

Figure 9. The two views of the d_{norm} Hirshfeld surface mapping within the range −0.0195 to 1.7591 arbitrary units for [In(Tm^{tBu})$_2$](InCl$_4$): (**a**) In1-cation, (**b**) In2-cation, and (**c**) In3-anion, with the close contacts indicated by the corresponding red dots on the surfaces with their intensity relative to the contact distance.

In addition to the close contacts as identified through the direct observation of red spots on the Hirshfeld surface of [In(Tm^{tBu})$_2$](InCl$_4$), two other important contacts, specifically In3–Cl1···π(pyrazolyl) and C1–H1b···In3, are detected based on the complementarity of shape as indicated by the hollows and bumps on the shape index mapped over the Hirshfeld surfaces between the independent In1 cation and In3 anion, despite the observation that the contact distances between Cl1 and the closest carbon atom of the five-membered imidazole ring, i.e., Cl1···C14, as well as H1b···In3, are longer than the corresponding ΣvdW, Figure 10.

Quantification of the close contacts in each individual component of [Tl^{I}(Tm^{tBu})]$_2$·2H$_2$O and [In^{III}(Tm^{tBu})$_2$](InCl$_4$) was performed through two-dimensional fingerprint plot analysis. The overall and delineated fingerprint plots for the individual components profiled in [Tl(Tm^{tBu})]$_2$·2H$_2$O, namely the Tm^{tBu} fragment, the water molecule, the thallium atom as well as the [Tl(Tm^{tBu})]$_2$ dimer, are illustrated in Figure 11. The fingerprint profiles for both Tm^{tBu} and [Tl(Tm^{tBu})]$_2$ resemble each other and have the shape of a flying fox, while those for H$_2$O and Tl display a cicada- and pincer-like profile, respectively. The decomposition of the corresponding overall profiles for Tm^{tBu} and [Tl(Tm^{tBu})]$_2$ show that their close contacts are dominated by H···H (69.5 and 76.6%, respectively), H···S/S···H (12.8 and 9.8%), H···C/C···H (6.2 and 6.6%), H···Tl/Tl···H (3.7 and 3.3%), S···Tl (for Tm^{tBu} only, 2.9%), and H···O/O···H (2.3 and 2.6%) as well as by other minor contacts that constitute less than 1.0% of all surface contacts, including H···N/N···H, S···O, and others. Among those contacts, only S···H, C···H, H···Tl/Tl···H, and O···H feature a distinctive tip with $d_i + d_e$ values corresponding to O1w–H1w···S2, O1w–H2w···C19, B1–H1···Tl/C10–H10a···Tl, and C13–H13···O1w, while the rest of the contacts present indistinct profiles.

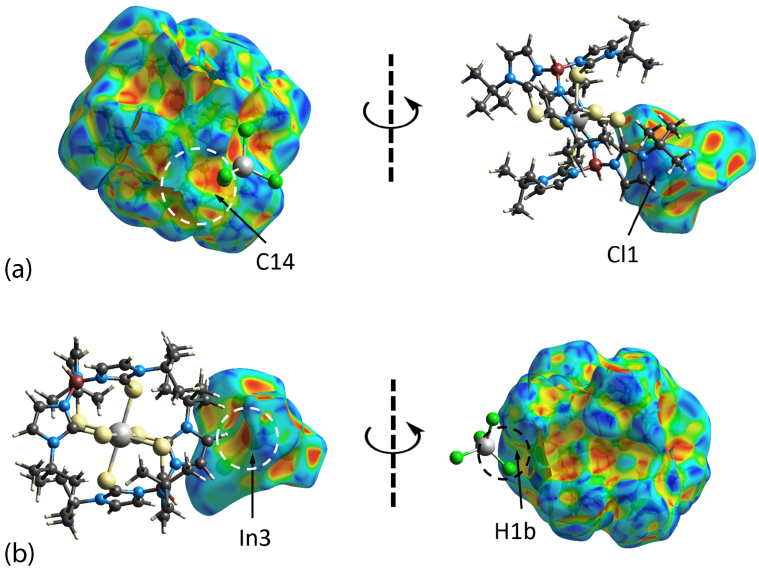

Figure 10. Two views of the shape-index mapped over the Hirshfeld surfaces for [In(Tm^{tBu})$_2$](InCl_4) within the property range −1.0 to +1.0 arbitrary units highlighting (**a**) In3–Cl1···π(C14) and (**b**) C1–H1b···In3 contacts, showing the shape complementarity as indicated by the hollow (orange) and bump (blue) on the surfaces.

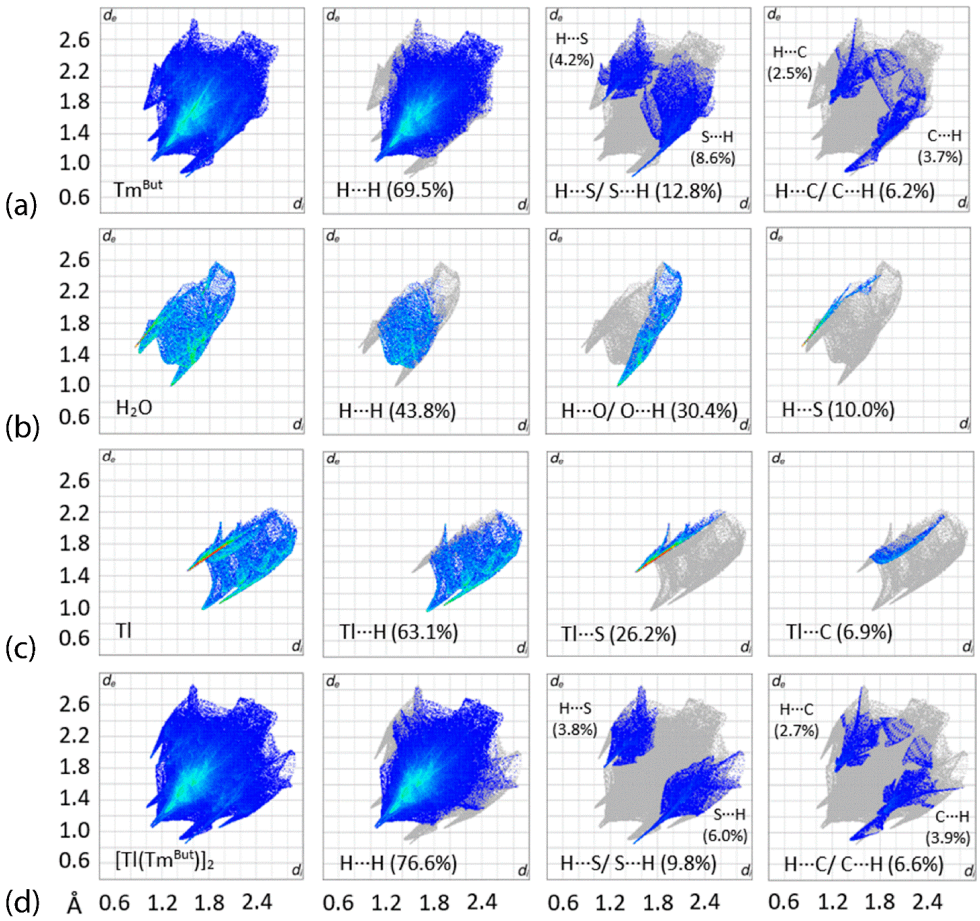

Figure 11. The overall two-dimensional fingerprint and decomposed plots delineated into the major contacts along with the percentage distributions for (**a**) Tm^{tBu}, (**b**) H_2O molecule, (**c**) thallium center, and (**d**) [Tl(Tm^{tBu})]$_2$ dimer for [Tl(Tm^{tBu})]$_2$·2H_2O.

As for the H_2O molecule and thallium atom, the major contacts for the former appear in the order H···H (43.8%) > O···H (30.4%) > H···S (10.0%) > H···C (7.2%) > H···N (6.2%) > O···S (2.5%), while the latter is dominated by H···Tl (63.1%) > S···Tl (26.2%) > C···Tl (6.9%) > N···Tl (3.9%). The $d_i + d_e$ distances associated with the significant peaks in these profiles correspond to the reciprocal contacts as identified in the Tm^{tBu} and $[Tl(Tm^{tBu})]_2$ profiles.

The overall and selected delineated two-dimensional fingerprint plots for the In1- and In2-cations as well as the In3-anion in $[In(Tm^{tBu})_2](InCl_4)$ are presented in Figure 12. As a general observation, the In1- and In2-cations exhibit a paw-like overall profile, which can be delineated mainly into H···H, H···Cl, and H···C/C···H contacts that constitute more than 93% of the Hirshfeld surfaces in each case. Specifically, the plots of the H···Cl contacts for the In1- and In2-cations display a distinctive spike in their decomposed fingerprint plots comprising 13–14% of all surface contacts with $d_i + d_e$ tipped at about 2.70 Å, which can be, respectively, attributed to H1b···Cl4 and H42···Cl4. The (inner)-C···H-(outer) and (inner)-H···C-(outer) contacts, represented by the pair of pincer-like profiles in the decomposed H···C/C···H fingerprint plots for the In1- and In2-cations, are due to H35···C19, with both constituting about 5% of the Hirshfeld surfaces with a $d_i + d_e$ distance of 2.76 Å, while the reciprocal (inner)-H···C-(outer) of the In1-cation and (inner)-C···H-(outer) of the In2-cation contribute 4.3 and 5.4%, respectively, to the contact surfaces but with a less significant $d_i + d_e$ distance, being longer than ΣvdW. A distinct feature is observed in the decomposed H···H fingerprint plot for the In2-cation compared to that for the In1-cation, in that for the former, a relatively prominent tip at $d_i + d_e$ = 1.93 Å is assignable to H37c···H30a.

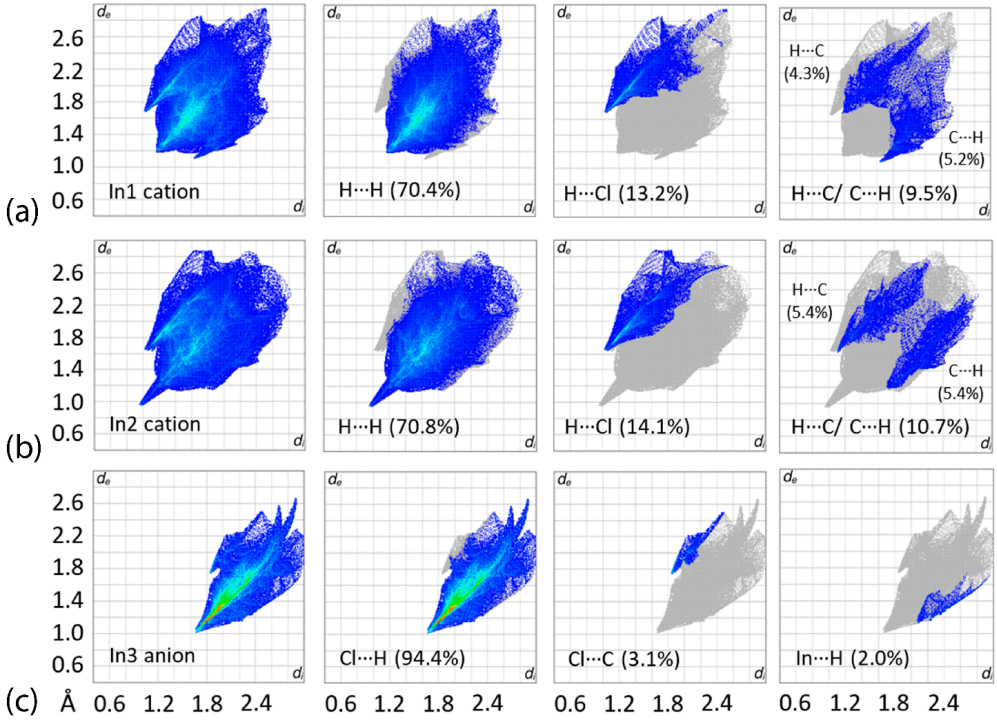

Figure 12. The overall two-dimensional fingerprint and decomposed plots delineated into the major contacts along with the percentage distributions for (**a**) In1-cation, (**b**) In2-cation, and (**c**) In3-anion for $[In(Tm^{tBu})_2](InCl_4)$.

On the other hand, the decomposition of the squid-like overall fingerprint plot for the In3-anion shows that about 94.4% of the contact surfaces are dominated by Cl···H with a $d_i + d_e$ distance tipped at 2.66 Å ascribed to the close C41–H41···Cl3 contact, while other minor contacts include Cl···C and In···H, which contribute about 3.1 and 2.0%, respectively, to the total surface, both with $d_i + d_e$ tips arising from the In3–Cl1···π(C14) and C1–H1b···In3 contacts as discussed above.

4. Conclusions

The synthesis, spectroscopic and X-ray crystallographic characterizations of two main group element complexes of a soft S_3-tripod-type ligand have been described. S_4-seesaw and S_6-flatenened octahedral geometries were found for the central atoms in $Tl(Tm^{tBu})]_2{\cdot}2H_2O$ and $[In(Tm^{tBu})_2](InCl_4)$, respectively. The analyses of the calculated Hirshfeld surfaces confirmed the geometric analysis of the molecular packing. These results suggest soft S_3-tripod-type ligands related to that discussed herein are a potentially useful class of ligands for coordination to *p*-block elements. The coordination of sulfur atoms gives rise to distinct electronic characteristics compared with the well-known hard N_3-type ligands. Therefore, the present chemistry paves the way for new coordination chemistry based on soft S_3-tripod-type ligands.

Supplementary Materials: The following supporting information can be downloaded at: https://www.mdpi.com/article/10.3390/cryst13050745/s1. Figure S1: IR spectra for $[Tl(Tm^{tBu})]_2{\cdot}2H_2O$ and $[In(Tm^{tBu})_2](InCl_4)$; Figure S2: FT-Raman spectra for $[Tl(Tm^{tBu})]_2{\cdot}2H_2O$ and $[In(Tm^{tBu})_2](InCl_4)$; Figure S3: ^{1}H-NMR spectrum of $[Tl^{I}(Tm^{tBu})]_2{\cdot}2H_2O$; Figure S4: ^{1}H-NMR spectrum for $[In^{III}(Tm^{tBu})_2](InCl_4)$; Figure S5: ^{13}C-NMR spectrum of $[In^{III}(Tm^{tBu})_2](InCl_4)$; Figure S6: UV–Vis spectra for $[Tl(Tm^{tBu})]_2{\cdot}2H_2O$ and $[In(Tm^{tBu})_2](InCl_4)$.

Author Contributions: Investigation, formal analysis, A.K. Investigation, formal analysis, writing—original draft preparation, writing—review and editing, K.F., S.L.T. and E.R.T.T. All authors have read and agreed to the published version of the manuscript.

Funding: This research was funded by an Ibaraki University Priority Research Grant and by the Joint Usage/Research Center for Catalysis (proposals 22DS0143 and 23DS0198).

Data Availability Statement: Crystallographic datasets for the structures $[Tl(Tm^{tBu})]_2{\cdot}2H_2O$ and $[In(Tm^{tBu})_2](InCl_4)$ are available through the Cambridge Structural Database with deposition numbers CCDC 2253015 ($[Tl(Tm^{tBu})]_2{\cdot}2H_2O$) and 2253016 ($[In(Tm^{tBu})_2](InCl_4)$). These data can be obtained free of charge via https://www.ccdc.cam.ac.uk/structures/ (accessed on 31 March 2023).

Conflicts of Interest: The authors declare no conflict of interest.

References

1. Trofimenko, S. *Scorpionates: The Coordination Chemistry of Polypyrazolylborate Ligands*; Imperial College Press: London, UK, 1999.
2. Pettinari, C. *Scorpionates II: Chelating Borate Ligands—Dedicated to Swiatoslaw Trofimenko*; Imperial College Press: London, UK, 2008.
3. Fujisawa, K.; Tobita, K.; Sakuma, S.; Savard, D.; Leznoff, D.L. Binuclear and mononuclear copper(II) chlorido complexes with hindered neutral N3 type ligands: Influence of ligand framework and charge on their structure and physicochemical properties. *Inorg. Chim. Acta* **2019**, *486*, 582–588. [CrossRef]
4. Lehnert, N.; Fujisawa, K.; Camarena, S.; Dong, H.T.; White, C.J. Activation of non-heme iron-nitrosyl complexes: Turning up the heat. *ACS Catal.* **2019**, *9*, 10499–10518. [CrossRef]
5. Fujisawa, K.; Ono, T.; Okamura, M. Synthesis and characterization of catecholato copper(II) complexes with sterically hindered neutral and anionic N3 type ligands: Tris(3,5-diisopropyl-1-pyrazolyl)methane and hydrotris(3,5-diisopropyl-1-pyrazolyl)borate. *Inorganics* **2020**, *8*, 37. [CrossRef]
6. Fujisawa, K.; Sakuma, S.; Ikarugi, R.; Jose, A.; Solomon, E.I. Thermally stable manganese(III) peroxido complexes with hindered N3 tripodal ligands: Structures and their physicochemical properties. *J. Inorg. Biochem.* **2021**, *225*, 111597. [CrossRef]
7. Trofimenko, S. Scorpionates: Genesis, milestones, prognosis. *Polyhedron* **2004**, *23*, 197–203. [CrossRef]
8. Lennartson, A. Toxic thallium. *Nat. Chem.* **2015**, *7*, 610–611. [CrossRef]
9. Renouf, C. A touch of indium. *Nat. Chem.* **2012**, *4*, 862. [CrossRef]
10. Fujisawa, K.; Kuboniwa, A.; Kiss, M.; Szilagyi, R.K. Mono- and binuclear tris(3-tert-butyl-2-sulfanylidene-1H-imidazol-1-yl)hydroborate bismuth(III) dichloride complexes: A soft scorpionate ligand can coordinate to p-block elements. *Acta Crystallogr. Sect. C Struct. Chem.* **2016**, *72*, 768–776. [CrossRef]
11. Steel, G.; Rajasekharan-Nair, R.; Stepek, I.A.; Kennedy, A.R.; Reglinski, J.; Spicer, M.D. Observations on the steric impact of N- and S-donor scorpionate ligands. *Eur. J. Inorg. Chem.* **2016**, *2016*, 2409–2412. [CrossRef]
12. Reglinski, J.; Spicer, M.D. Chemistry of the p-block elements with anionic scorpionate ligands. *Coord. Chem. Rev.* **2015**, *297–298*, 181–207. [CrossRef]
13. Spicer, M.D.; Reglinski, J. Soft scorpionate ligands based on imidazole-2-thione donors. *Eur. J. Inorg. Chem.* **2009**, *2009*, 1553–1574. [CrossRef]

14. Rong, Y.; Palmer, J.H.; Parkin, G. Benzannulated tris(2-mercapto-1-imidazolyl)hydroborato ligands: Tetradentate κ^4-S_3H binding and access to monomeric monovalent thallium in an [S_3] coordination environment. *Dalton Trans.* **2014**, *43*, 1397–1407. [CrossRef]
15. Yurkerwich, K.; Buccella, D.; Melnick, J.G.; Parkin, G. Monovalent indium in a sulfur-rich coordination environment: Synthesis, structure and reactivity of tris(2-mercapto-1-tert-butylimidazolyl)hydroborato indium, [Tm^{But}]In. *Chem. Commun.* **2008**, *28*, 3305–3307. [CrossRef]
16. Kimblin, C.; Bridgewater, B.M.; Hascall, T.; Parkin, G. The synthesis and structural characterization of bis(mercaptoimidazolyl)(pyrazolyl)hydroborato and tris(mercaptoimidazolyl)hydroborato complexes of thallium(I) and thallium(III). *J. Chem. Soc. Dalton Trans.* **2000**, 1267–1274. [CrossRef]
17. Ojo, J.F.; Slavin, P.A.; Reglinski, J.; Garner, M.; Spicer, M.D.; Kennedy, A.R.; Teat, S.J. The synthesis of soft tripodal ligands: Restrictions on the preparation of hydrotris(thiazolyl)borate anions from borohydride melts. *Inorg. Chim. Acta* **2001**, *313*, 15–20. [CrossRef]
18. Slavin, P.A.; Reglinski, J.; Spicera, M.D.; Kennedy, A.R. Preparation and crystal structure of the [bis{hydrotris(methimazolyl)borato}thallium(III)] cation: Modulated chemistry resulting from the use of soft and hard tripodal ligands. *J. Chem. Soc. Dalton Trans.* **2000**, 239–240. [CrossRef]
19. Yurkerwich, K.; Yurkerwich, M.; Parkin, G. Synthesis and structural characterization of tris(2-mercapto-1-adamantylimidazolyl)hydroborato complexes: A sterically demanding tripodal [S_3] donor ligand. *Inorg. Chem.* **2011**, *50*, 12284–12295. [CrossRef]
20. Dodds, C.A.; Reglinski, J.; Spicer, M.D. Lower main-group element complexes with a soft scorpionate ligand: The structural influence of stereochemically active lone pairs. *Chem. Eur. J.* **2006**, *12*, 931–939. [CrossRef]
21. Armarego, W.L.F.; Chai, C.L.L. *Purification of Laboratory Chemicals*, 7th ed.; Butterworth-Heinemann: Oxford, UK, 2012.
22. Kreider-Mueller, A.; Rong, Y.; Owen, J.S.; Parkin, G. Molecular structures of tris(2-mercapto-1-tert-butylimidazolyl)hydroborato and tris(2-mercapto-1-adamantylimidazolyl)hydroborato sodium complexes: Analysis of [Tm^R] ligand coordination modes and conformations. *Dalton Trans.* **2014**, *43*, 10852–10865. [CrossRef]
23. Mihalcik, D.J.; White, J.L.; Tanski, J.M.; Zakharov, L.N.; Yap, G.P.A.; Incarvito, C.D.; Rheingold, A.L.; Rabinovich, D. Cobalt tris(mercaptoimidazolyl)borate complexes: Synthetic studies and the structure of the first cobaltaboratrane. *Dalton Trans.* **2004**, 1626–1634. [CrossRef]
24. Kimblin, C.; Bridgewater, B.M.; Churchill, D.G.; Parkin, G. Mononuclear tris(2-mercapto-1-arylimidazolyl)hydroborato complexes of zinc, [Tm^{Ar}]ZnX: Structural evidence that a sulfur rich coordination environment promotes the formation of a tetrahedral alcohol complex in a synthetic analogue of LADH. *Chem. Commun.* **1999**, 2301–2302. [CrossRef]
25. Reglinski, J.; Garner, M.; Cassidy, I.D.; Slavin, P.A.; Spicer, M.D.; Armstrong, D.R. Sodium hydrotris(methimazolyl)borate, a novel soft, tridentate ligand: Preparation, structure and comparisons with sodium hydrotris(pyrazolyl)borate. *J. Chem. Soc. Dalton Trans.* **1999**, 2119–2126. [CrossRef]
26. *Rigaku Oxford Diffraction, CrysAlis PRO*; Oxford Diffraction Ltd.: Oxfordshire, UK, 2015.
27. Sheldrick, G.M. A short history of SHELX. *Acta Crystallogr. Sect. A Found. Crystallogr.* **2008**, *64*, 112–122. [CrossRef] [PubMed]
28. Sheldrick, G.M. Crystal structure refinement with SHELXL. *Acta Crystallogr. Sect. C Struct. Chem.* **2015**, *71*, 3–8. [CrossRef] [PubMed]
29. Farrugia, L.J. WinGX and ORTEP for Windows: An update. *J. Appl. Crystallogr.* **2012**, *45*, 849–854. [CrossRef]
30. Brandenburg, K. *DIAMOND, Crystal Impact GbR*; Crystal Impact GbR: Bonn, Germany, 2006.
31. Spek, A.L. checkCIF validation ALERTS: What they mean and how to respond. *Acta Crystallogr. Sect. E Crystallogr. Commun.* **2020**, *76*, 1–11. [CrossRef]
32. Yang, L.; Powell, D.R.; Houser, R.P. Structural variation in copper(I) complexes with pyridylmethylamide ligands: Structural analysis with a new four-coordinate geometry index, τ_4. *Dalton Trans.* **2007**, 955–964. [CrossRef]
33. Schollmeyer, D.; Shishkin, O.V.; Rühl, T.; Vysotsky, M.O. OH–π and halogen–π interactions as driving forces in the crystal organisations of tri-bromo and tri-iodo trityl alcohols. *CrystEngComm* **2008**, *10*, 715–723. [CrossRef]
34. Spackman, P.R.; Turner, M.J.; McKinnon, J.J.; Wolff, S.K.; Grimwood, D.J.; Jayatilaka, D.; Spackman, M.A. CrystalExplorer: A program for Hirshfeld surface analysis, visualization and quantitative analysis of molecular crystal. *J. Appl. Crystallogr.* **2021**, *54*, 1006–1011. [CrossRef]
35. Tan, S.L.; Jotani, M.M.; Tiekink, E.R.T. Utilizing Hirshfeld surface calculations, non-covalent inter action (NCI) plots and the calculation of inter action energies in the analysis of molecular packing. *Acta Crystallogr. Sect. E Crystallogr. Commun.* **2019**, *75*, 308–318. [CrossRef]
36. Spackman, M.A.; Jayatilaka, D. Hirshfeld surface analysis. *CrystEngComm* **2009**, *11*, 19–32. [CrossRef]